Cooperative ordering of holes and spins in $La_2NiO_{4.125}$

J. M. Tranquada and J. E. Lorenzo*
Physics Department, Brookhaven National Laboratory, Upton, New York 11973

D. J. Buttrey and V. Sachan
Department of Chemical Engineering, University of Delaware, Newark, Delaware 19716
(Received 22 February 1995)

$La_2NiO_{4.125}$ exhibits a cooperative ordering of dopant-induced holes and Ni spins below a transition temperature of 110 K. There is also an ordering of interstitial oxygens that occurs near room temperature. We present a comprehensive analysis of experimentally observed superlattice intensities in terms of structural models, justifying previous identifications. The model for the interstitial order involves a $3\mathbf{a} \times 5\mathbf{b} \times 5\mathbf{c}$ unit cell with an ideal interstitial density of $\delta = \frac{2}{15}$ per formula unit. In the spin and charge ordered state, the magnetic moments are sinusoidally modulated within the NiO_2 planes. The moments point transverse to the modulation direction, with nearest neighbors antiparallel, and have a maximum amplitude that is $> 80\%$ of that observed in undoped La_2NiO_4. A corresponding modulation of atomic positions within NiO_2 planes involves breathing-mode distortions consistent with a modulation of the charge density. The results are compared with theoretical models and with experimental observations on related systems.

I. INTRODUCTION

The behavior of holes doped into a two-dimensional antiferromagnet has been the subject of numerous theoretical investigations in the last few years. Emery and Kivelson[1–3] have emphasized the tendency of neutral holes in an antiferromagnet to phase separate, and they have proposed that the frustration of macroscopic phase separation by long-range Coulomb interactions is responsible for many of the unusual properties of the layered copper-oxide superconductors. One particular type of microscopic phase separation that has been found in both mean-field[4–9] and variational Monte Carlo[10,11] studies of the two-dimensional Hubbard model involves the localization of holes in domain walls within an antiferromagnetic background.

We recently reported[12] that such a phase is physically realized in $La_2NiO_{4+\delta}$ with $\delta = 0.125$. Below 110 K the domain walls order periodically and act as antiphase domain boundaries for the magnetic structure. The relevance of the Hubbard model studies to understanding the nickelate has been unclear since a single-band Hubbard model properly describes a spin-$\frac{1}{2}$ system while Ni is spin 1. However, Zaanen and Littlewood[13] have now presented multiband-Hubbard-model calculations appropriate for an NiO_2 plane which show the same type of domain wall structures. Their analysis shows that these features, which are driven by purely electronic interactions, are stabilized by electron-phonon coupling in the nickelate.

The identification of spin and charge order in $La_2NiO_{4.125}$ is complicated to some extent by the occurrence of ordering among the interstitial oxygens. In the present paper we justify our previous identifications by performing a comprehensive analysis of the ordering of the interstitials, which occurs near room temperature, as well as the spin and breathing-type lattice modulations that occur at low temperature. The ordering of the interstitials causes lattice distortions with which the charge and spin order must compete; however, the atomic displacements involved in the two types of order are quite different in nature.

The rest of the paper is arranged as follows. The experimental details are given in the next section, followed by a general description of the superlattice peaks that are observed. The analysis of the interstitial order is presented in Sec. IV, and that for the cooperative spin and lattice modulations appears in Sec. V. A discussion of the results, with a comparison to theory and to related systems, is followed by a summary. The structure factors for the ordered interstitials are described in the Appendix.

II. EXPERIMENTAL PROCEDURES

The 1.3 g crystal used in the present study is the same one that we used in our original work.[12] It was obtained from a boule grown by rf induction skull melting.[14] The oxygen concentration was selected by annealing at 700 °C in 1 atm O_2 for several hours, followed by a quench to room temperature. The proper annealing conditions had been determined previously in the study by Rice and Buttrey.[14] The value of δ was checked by iodometric analysis of other material prepared in the same anneal. The lattice parameters determined by neutron diffraction at 10 K are $a = 5.457$ Å and $c = 12.62$ Å.

The neutron diffraction measurements were performed on the H4M and H8 triple-axis spectrometers at the High Flux Beam Reactor located at Brookhaven National Lab-

oratory. The (002) reflection of pyrolytic graphite (PG) was used for the monochromator and analyzer, together with a PG filter in the incident beam to eliminate $\lambda/2$ contamination. A neutron energy of 14.7 meV was utilized for all measurements. The sample temperature was controlled with a Displex closed-cycle He refrigerator.

The crystal was initially oriented in the $(h0l)/(0kl)$ zone (see below for a discussion of twinning), and was later reoriented to access the $(hk0)$ zone. Integrated Bragg peak intensities were determined at a temperature of 10 K from θ-2θ scans, with typical collimations of 40′-20′-20′-40′. Measurements in different orientations were normalized using reflections that are accessible in both zones. For each set of measurements, the sample was slowly cooled between 300 K and 240 K to enhance the ordering of the oxygen interstitials.

III. GENERAL DESCRIPTION

We observe two types of ordering in $La_2NiO_{4.125}$: one corresponding to ordering of the oxygen interstitials and another involving ordering of the doped holes and the Ni spins. (The justification for this assertion will be developed below.) The ordering of the interstitials is indicated by the appearance of two distinct sets of superlattice peaks, as depicted in Fig. 1. Each set of peaks is characterized by a modulation wave vector $\mathbf{g}_j$ such that if $\mathbf{Q}_{SL}$ is the position of a superlattice peak, then

$$\mathbf{Q}_{SL} = \mathbf{G} \pm \mathbf{g}_j, \tag{1}$$

where $\mathbf{G}$ is a reciprocal lattice vector corresponding to the fundamental tetragonal unit cell containing two formula units (K_2NiF_4 structure). At this point we note that, while we chose to reference the structural modulations to the fundamental cell, it will be more convenient notationally to make use of indexing based on the orthorhombic cell specified by $\sqrt{2}\mathbf{a} \times \sqrt{2}\mathbf{b} \times \mathbf{c}$ relative to the tetragonal. The two wave vectors $\mathbf{g}_j$ both specify modulations within the NiO_2 planes, and it seems most sensible to assume that they are in orthogonal directions. Since we have not resolved an orthorhombic splitting, we arbitrarily assign the (h,k) directions of the modulations as follows:

$$\mathbf{g}_1 = \left(\frac{1}{3}, 0, 1\right) \tag{2}$$

and

$$\mathbf{g}_2 = \left(0, \frac{4}{5}, \frac{4}{5}\right). \tag{3}$$

The existence of twin domains rotated by 90° with respect to one another would then explain why both sets of peaks appear to occur in the same zone of reciprocal space. The two sets of domains are indicated in Fig. 1 by different shadings. A second type of twinning is associated with $\mathbf{g}_2$. Related, but inequivalent, domains are characterized by

$$\mathbf{g}_2' = \left(0, -\frac{4}{5}, \frac{4}{5}\right). \tag{4}$$

The relationship between the $\mathbf{g}_2$ and $\mathbf{g}_2'$ domains will become clearer after we describe the structural model in the next section. The $\mathbf{g}_1$ peaks were first observed by Yamada *et al.*;[15] however, they did not report seeing the $\mathbf{g}_2$ (and $\mathbf{g}_2'$) reflections. We have also observed very weak second harmonic peaks of both types.

With two distinct sets of superlattice peaks, one might be tempted to assign each to a different phase. The fact that they appear at precisely the same temperature could be explained by phase separation. However, certain behaviors of the peak intensities with temperature strongly suggest that the two sets are both associated with a single phase. First of all, close to the transition temperature, the peak intensities show a rather sluggish time dependence following a temperature change, very similar to the slow ordering kinetics that we have documented[16,17] in $La_2NiO_{4+\delta}$ with $0.05 \lesssim \delta \lesssim 0.11$. On warming, the peaks

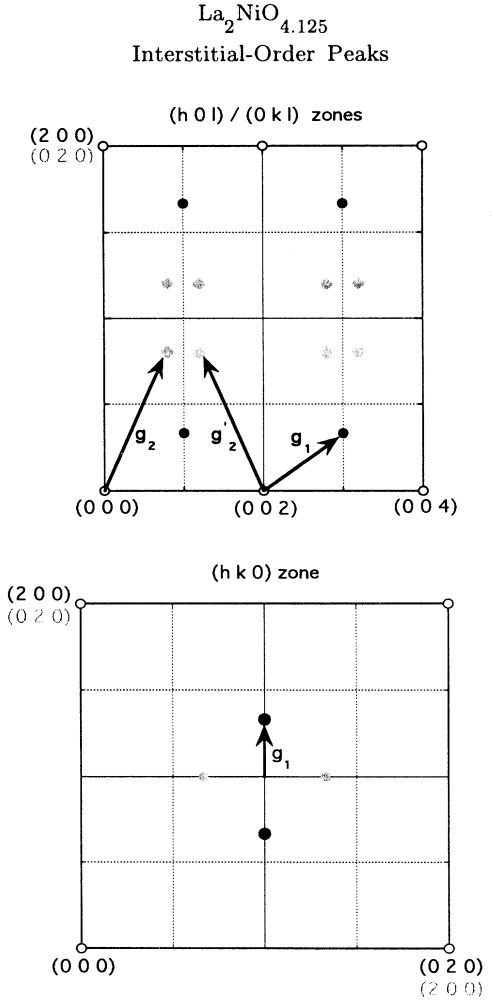

FIG. 1. Schematic diagrams indicating locations of superlattice peaks corresponding to ordering of the oxygen interstitials in the $(h0l)/(0kl)$ and $(hk0)$ zones of reciprocal space.

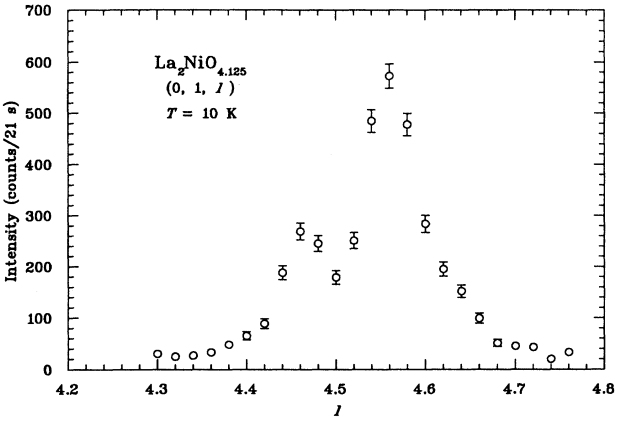

FIG. 2. Example of diffuse scattering measured along $(0,1,l)$ at 10 K.

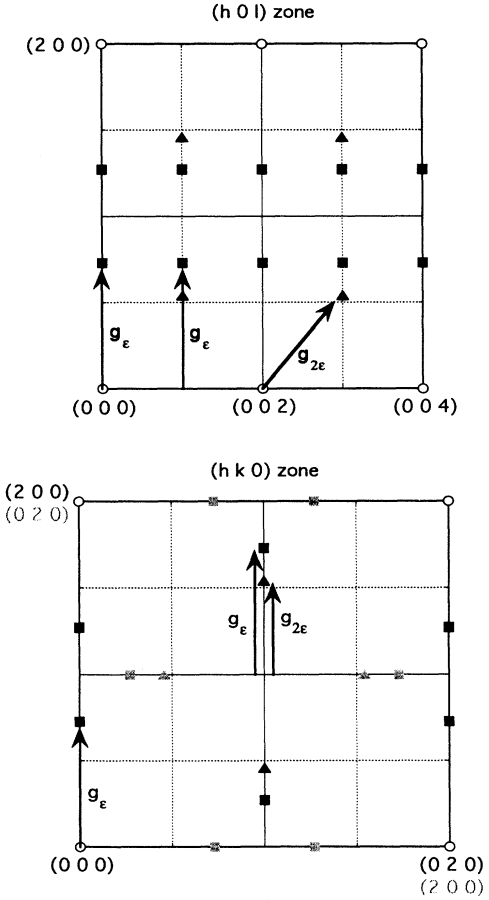

FIG. 3. Schematic diagrams indicating locations of superlattice peaks corresponding to spin and charge ordering in the $(h0l)$ and $(hk0)$ zones of reciprocal space.

disappear near 310 K, while on cooling, they reappear at 300 K after waiting at least 1 h at that temperature. As shown previously,[12] cooling the sample rapidly from $T \gtrsim 310$ K to < 250 K leads to a substantially weaker superlattice intensity than that obtained after slow cooling. The important point is that the two sets of reflections show the same relative changes in intensity with temperature and cooling rate. To us this behavior indicates a single ordered phase. Also, we will present below a model for the oxygen ordering that is consistent both with the two modulation wave vectors and with the known concentration of interstitials.

Besides the superlattice peaks, there also exists weak diffuse scattering, which indicates that a small fraction of the interstitials do not participate in the three-dimensional (3D) ordering. Figure 2 shows an example of the diffuse signal. It is similar to the type of scattering observed[16] in $La_2NiO_{4+\delta}$ with $0.05 \lesssim \delta \lesssim 0.11$, where the interstitials order one-dimensionally in a staged fashion. The diffuse signal may come from regions between the dominant domains of 3D order.

The combined ordering of charges and spins does not occur until the crystal is cooled below 110 K. The positions of the corresponding superlattice peaks are indicated in Fig. 3, and representative scans through some of these peaks are shown in Fig. 4. The magnetic peaks are characterized by the modulation wave vector

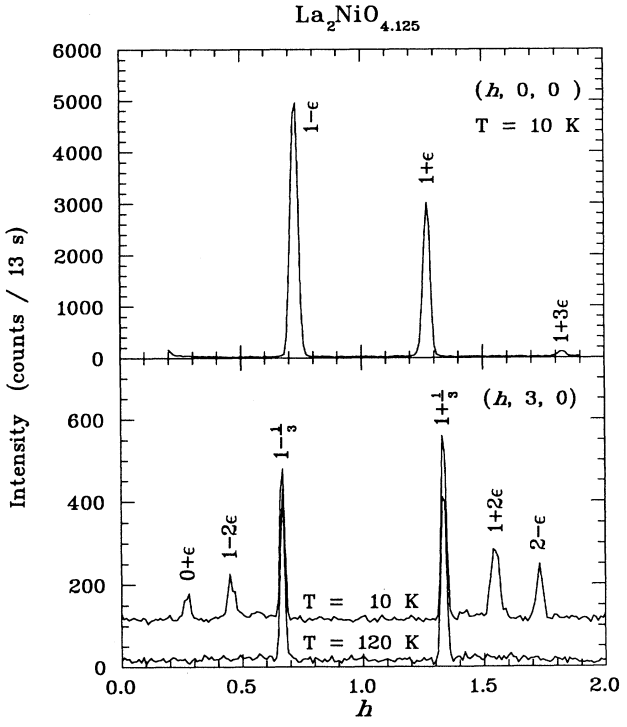

FIG. 4. Selected scans in the $(hk0)$ zone through $\mathbf{g}_1$-, $\mathbf{g}_\epsilon$-, $\mathbf{g}_{2\epsilon}$-, and $\mathbf{g}_{3\epsilon}$-type superlattice peaks. The lower panel shows scans below and above the spin-and-charge-ordering transition at 110 K. The 10 K scan has been shifted vertically for clarity.

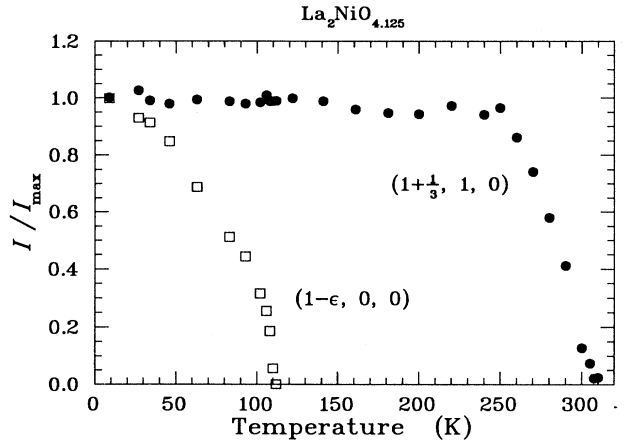

FIG. 5. Temperature dependence of the normalized integrated intensities for a $\mathbf{g}_1$ and a $\mathbf{g}_\epsilon$ peak.

$$\mathbf{g}_\epsilon = (1-\epsilon, 0, 0), \tag{5}$$

while for the charge-ordering peaks we find

$$\mathbf{g}_{2\epsilon} = (2\epsilon, 0, 1). \tag{6}$$

The value of ϵ is temperature dependent,[12] varying from 0.295 at 110 K to 0.271 at 10 K. There is one difference in applying Eq. (1) to the magnetic peaks: the relative phases of the modulations associated with the magnetic moments in the two NiO_2 layers per unit cell make the moments on the two different Ni sites of the unit cell inequivalent. Thus, for the magnetic structure the face-centered symmetry of the orthorhombic cell is broken, so that the usual restriction on $\mathbf{G} = (h, 0, l)$ that both h and l must be even is changed to h even and l integer. Furthermore, we also observe third-harmonic magnetic peaks described by

$$\mathbf{g}_{3\epsilon} = (1-3\epsilon, 0, 0). \tag{7}$$

Again, Yamada *et al.*[15] observed the $\mathbf{g}_\epsilon$ and $\mathbf{g}_{3\epsilon}$ reflections, but did not find the $\mathbf{g}_{2\epsilon}$ peaks.

The wave vectors $\mathbf{g}_1$ and $\mathbf{g}_{2\epsilon}$ are quite similar in form. If they represented similar structural modulations, then one might expect to see a change in intensity of $\mathbf{g}_1$ peaks when the charge and spin ordering occurs. Figure 5 shows the temperature dependence observed for $(1+\frac{1}{3}, 1, 0)$ and $(1-\epsilon, 0, 0)$ reflections. No significant correlation of the intensities is observed.

IV. ANALYSIS OF INTERSTITIAL ORDER

The unit cell required to describe the interstitial ordering is $3 \times 5 \times 5$ relative to an orthorhombic unit cell containing four formula units. In general, there would be many free parameters required to describe the atomic positions within such a unit cell, and without severe constraints on these parameters, one would predict intensity at many new superlattice positions where none is observed experimentally. Ignoring the interstitials for a moment, a more convenient way in which to describe the atomic displacements associated with the ordering is in terms of an incommensurate modulation of the structure, as we discuss below.

We begin by writing the structure factor F_n for the nth unit cell (containing two formula units), located at $\mathbf{R}_n$, as

$$F_n(\mathbf{Q}) = \sum_j b_j e^{-\mathbf{Q}\cdot\mathbf{r}_{nj}}, \tag{8}$$

where b_j is the neutron scattering length for the jth atom in the unit cell. In general, the displacements can be written

$$\mathbf{r}_{nj} = \mathbf{r}_j + \delta\mathbf{r}_{nj}, \tag{9}$$

with

$$\delta\mathbf{r}_{nj} = \mathbf{c}_j \cos(\mathbf{g}\cdot\mathbf{R}_n) + \mathbf{s}_j \sin(\mathbf{g}\cdot\mathbf{R}_n). \tag{10}$$

Plugging these formulas into Eq. (8) and expanding the exponential, one finds, in the limit of small displacements, that

$$\delta F_n = f_c(\mathbf{Q}) \cos(\mathbf{g}\cdot\mathbf{R}_n) + f_s(\mathbf{Q}) \sin(\mathbf{g}\cdot\mathbf{R}_n), \tag{11}$$

where

$$\begin{aligned} f_c(\mathbf{Q}) &= -i \sum_j b_j (\mathbf{Q}\cdot\mathbf{c}_j) e^{-i\mathbf{Q}\cdot\mathbf{r}_j} \\ &= f_c' + i f_c'', \end{aligned} \tag{12}$$

and f_s is similarly defined. Using methods described by Scaringe and Comés,[18] one can then show that the scattered intensity for superlattice peaks is given by

$$\begin{aligned} I = N^2 \sum_{\mathbf{G}} \{ & |F_+|^2 \delta[\mathbf{Q} - (\mathbf{G} + \mathbf{g})] \\ & + |F_-|^2 \delta[\mathbf{Q} - (\mathbf{G} - \mathbf{g})] \}, \end{aligned} \tag{13}$$

where

$$|F_\pm|^2 = \frac{1}{4}\left[(f_c' \mp f_s'')^2 + (f_c'' \pm f_s')^2\right], \tag{14}$$

and we have assumed that the number of unit cells in the crystal, N, approaches infinity. For comparison, the intensities of the fundamental reflections are given by

$$I = N^2 \sum_{\mathbf{G}} |\langle F\rangle|^2 \delta(\mathbf{Q} - \mathbf{G}), \tag{15}$$

where

$$\begin{aligned} \langle F\rangle &= \frac{1}{N}\sum_n F_n \\ &= \sum_j b_j e^{-\mathbf{Q}\cdot\mathbf{r}_j}. \end{aligned} \tag{16}$$

Besides the displacements of atoms in the lattice, we must also consider scattering from the interstitials. While this contribution cannot be described by a single

sinusoidal factor, we show in the Appendix that it can be described as a sum of contributions to the fundamental, first harmonic, and second harmonic reflections. Thus, the contribution to the scattering amplitude for the first harmonic peaks has the same form as Eq. (11), and is readily included in the analysis of peak intensities. Note that we ignore Debye-Waller factors in our analysis because the measurements were performed at low temperature, and the maximum Q studied (4.8 Å^{-1}) is fairly small.

A. Fundamental reflections

The most direct information on the interstitial order comes from the superlattice peaks. While scattering from the interstitials and displacements affects the intensities of the Bragg peaks corresponding to the undistorted lattice, we choose to ignore this very small contribution in analyzing the fundamental reflections. The main purpose of evaluating their intensities is to obtain a scale factor so that the superlattice intensities can be put on an absolute scale.

Figure 6 shows the observed values of $|F|^2$ for eight fundamental reflections in the $(h0l)$ zone plotted versus the values calculated using the K_2NiF_4 structure. The only two parameters not determined by symmetry for this structure are the relative coordinates along the c axis of the apical oxygens (O_2 site) and the lanthanum ions. A least squares fit yielded the values $z_{O_2} = 0.157$ and $z_{La} = 0.353$, respectively. The fact that the points in the figure do not lie on a straight line is due to extinction, which we take into account by fitting the data with the formula

$$|F|^2_{\text{obs}} = \frac{A|F|^2_{\text{calc}}}{1 + a|F|^2_{\text{calc}}}. \tag{17}$$

The values of $|F|^2_{\text{obs}}$ for the superlattice peaks are all weak and in the region where extinction is negligible.

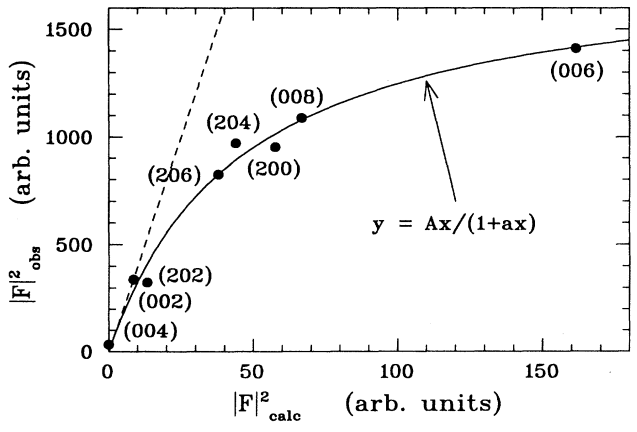

FIG. 6. Observed values of $|F|^2$ for fundamental Bragg peaks plotted as a function of the calculated ones. The solid line indicates the curve $y = Ax/(1 + ax)$, with fitted parameters $A = 40.0$ and $a = 0.022$. The dashed line indicates $y = Ax$.

B. $\mathbf{g}_2$ structure

We start with an analysis of the $\mathbf{g}_2$ reflections because they are similar to the superlattice peaks seen previously[16] in crystals with $0.05 \lesssim \delta \lesssim 0.11$. In the latter case the modulation wave vector can be written $\mathbf{g}_m = (0, 1, \frac{1}{m})$, where m is the order of the oxygen staging (i.e., the number of NiO_2 layers between interstitial-occupied La_2O_2 layers). The intensities of the superlattice peaks can be explained by the tilt pattern of the NiO_6 octahedra,[19,16] and no indication of a three-dimensional ordering of the interstitials has been observed by neutron diffraction.

At $\delta = 0.105$ we have observed a stage order of $m = 2$. With increasing oxygen concentration one might expect the next stage order to be $m = 1$. Instead, at $\delta = 0.125$ we find the $\mathbf{g}_2$ peaks, which indicate that the positions of the interstitials are correlated along the **b** and **c** directions. To gain some insight into the structure, we initially considered a model in which the octahedra are rotated and displaced in a rigid fashion. Consideration of the pattern of rotated octahedra determined by the wave vector $\mathbf{g}_2$ led to the model structure shown in Fig. 7. The interstitials are assumed to sit in the largest available openings. The density of interstitials per fundamental unit cell in this projection is $\frac{4}{5}$.

While the rigid-rotation model is useful for identifying the ordering pattern, we have found that, to obtain reasonable quantitative agreement with the observed superlattice intensities, it is necessary to allow for substantial distortions of the octahedra. We consider a fundamental unit cell containing Ni atoms at (0,0,0) and $(0, -\frac{1}{2}, \frac{1}{2})$, with identical displacements of the octahedral oxygens

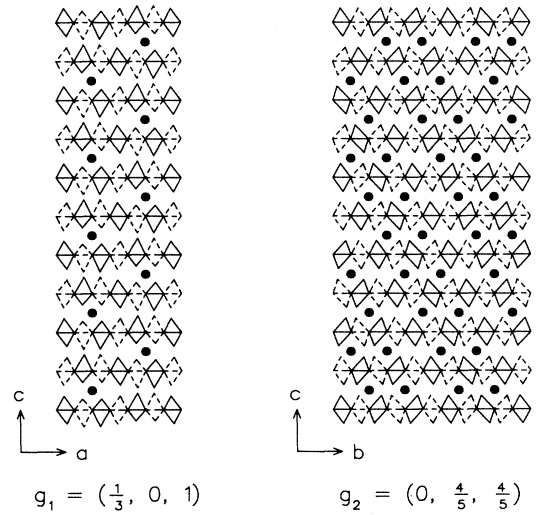

FIG. 7. Schematic model of the interstitial oxygen ordering in $La_2NiO_{4.125}$. The NiO_6 octahedra are depicted by diamonds, interstitials by solid circles. Octahedra drawn with solid lines are centered in the plane of the page, while those with dashed lines are half a lattice spacing above or below the page. (La ions are neglected for clarity.) The magnitudes of atomic displacements have been exaggerated. Interstitial positions are projected onto the plane. The ideal interstitial concentration corresponds to $\delta = \frac{2}{15}$.

about each site. [This is the cell for $\mathbf{g}_2$; for $\mathbf{g}_2'$, the second Ni site is at $(0, \frac{1}{2}, \frac{1}{2})$.] The largest displacements are those of the apical oxygens, Δy_{O_2}, which move in a rotating fashion about each Ni. The La ions in the same layer move by Δy_{La}. The in-plane oxygens also move in a manner corresponding to tilting of the octahedra; however, because neighboring octahedra are not rotated by equal and opposite amounts, we cannot expect the oxygens at $(\pm\frac{1}{4}, \frac{1}{4}, 0)$ and $(\pm\frac{1}{4}, -\frac{1}{4}, 0)$ to move by equal and opposite amounts. Instead, we include only the former pair of O_1 sites [and $(\pm\frac{1}{4}, -\frac{1}{4}, \frac{1}{2})$] in the unit cell.

The displacements depend on the position of the unit cell $\mathbf{R}_n$ in a sinusoidal fashion; e.g.,

$$\Delta y_{O_{2,n}} = \Delta y_{O_2} \sin(\mathbf{g}_2 \cdot \mathbf{R}_n + \phi), \tag{18}$$

where the parameter ϕ is necessary to specify the phase of the modulation with respect to a specific choice for the positions of the interstitials. Because of the unsymmetrical modeling of the O_1 displacements, we allow their modulation to be phase shifted with respect to the apical oxygens by using

$$\Delta z_{O_{1,n}} = \Delta z_{O_{1,s}} \sin(\mathbf{g}_2 \cdot \mathbf{R}_n + \phi) + \Delta z_{O_{1,c}} \cos(\mathbf{g}_2 \cdot \mathbf{R}_n + \phi). \tag{19}$$

The simplest way to express the model may be to write down the structure factors f_c and f_s defined in Eq. (11). The displacements of the two octahedra in the elemental cell are identical, so that each structure factor is equal to that for a single octahedron times the factor $1 + \exp[i\pi(k \mp l)]$ (with $-$ for $\mathbf{g}_2$, $+$ for $\mathbf{g}_2'$). The latter factor is always equal to 2 for the observed $(0kl)$ superlattice peaks. Now, because of the phase shift ϕ, we proceed to write down the structure factors in two steps. We first define the intermediate quantities $\tilde{f}_c$ and $\tilde{f}_s$:

$$\tilde{f}_c = i8\pi b_O l \Delta z_{O_{1,c}} e^{-i\frac{\pi}{2}k} \cos\left(\frac{\pi}{2}h\right), \tag{20}$$

$$\tilde{f}_s = -8\pi\Big[b_O k \Delta y_{O_2} \sin(2\pi z_{O_2} l) + i b_O l \Delta z_{O_{1,s}} e^{-i\frac{\pi}{2}k} \cos\left(\frac{\pi}{2}h\right) + b_{La} k \Delta y_{La} \sin(2\pi z_{La} l)\Big]. \tag{21}$$

In terms of these, one can then write

$$f_c = \tilde{f}_s \sin\phi + \tilde{f}_c \cos\phi, \tag{22}$$

$$f_s = \tilde{f}_s \cos\phi - \tilde{f}_c \sin\phi. \tag{23}$$

The contributions from the interstitials themselves are given in the Appendix.

In fitting the observed values of $|F|^2$, we have assumed that there are equal volumes of $\mathbf{g}_2$ and $\mathbf{g}_2'$ domains, and we have taken account of the fractional occupancy of the interstitial sites [the ideal δ is $\frac{2}{15}$ (≈ 0.133) for the model structure, as explained below]. The oxygen and lanthanum displacement parameters were adjusted to obtain the best least squares fit, taking into account the scale factor A determined in the analysis of the fundamental reflections. Reasonable fits were obtained with the phase ϕ set equal to $\frac{9}{10}\pi$ ($-\frac{9}{10}\pi$) for $\mathbf{g}_2$ ($\mathbf{g}_2'$) peaks. The results are shown in Table I and the corresponding displacement parameters are listed in Table II. We have not quoted error bars for the parameter values because we expect them to be dominated by systematic effects such as the lack of complete ordering of the interstitials.

While the agreement between $|F|^2_{obs}$ and $|F|^2_{calc}$ is far from perfect, the model does properly give strong peaks near (0,1,4) and (0,3,2), with very weak intensities elsewhere. Whereas the large values of $|F|^2$ are due pre-

TABLE I. Comparison of the observed values of $|F|^2$ with those calculated using the model discussed in the text for the $\mathbf{g}_2$ and $\mathbf{g}_2'$ superlattice peaks. Also included are the results calculated from the model assuming that (a) only the interstitials or (b) only the displacements contribute.

(h,k,l)	G+g	$\lvert F\rvert^2_{obs}$	$\lvert F\rvert^2_{calc}$	$\lvert F_{int}\rvert^2$	$\lvert F_{disp}\rvert^2$
(0,0.8,1.2)	$(0,0,2)+\mathbf{g}_2'$	0.13(2)	0.01	0.07	0.03
(0,0.8,2.8)	$(0,0,2)+\mathbf{g}_2$	0.03(2)	0.01	0.11	0.02
(0,0.8,4.8)	$(0,0,4)+\mathbf{g}_2$	1.61(4)	1.23	0.11	0.50
(0,0.8,5.2)	$(0,0,6)+\mathbf{g}_2'$	1.78(4)	1.41	0.07	0.97
(0,1.2,0.8)	$(0,2,0)-\mathbf{g}_2'$	0.01(2)	0.00	0.07	0.08
(0,1.2,1.2)	$(0,2,2)-\mathbf{g}_2$	0.03(2)	0.09	0.11	0.15
(0,1.2,2.8)	$(0,2,2)-\mathbf{g}_2'$	0.03(2)	0.00	0.07	0.10
(0,1.2,3.2)	$(0,2,4)-\mathbf{g}_2$	0.02(2)	0.01	0.11	0.14
(0,1.2,4.8)	$(0,2,4)-\mathbf{g}_2'$	1.51(4)	1.92	0.07	1.36
(0,1.2,5.2)	$(0,2,6)-\mathbf{g}_2$	1.13(4)	1.44	0.11	0.64
(0,2.8,0.8)	$(0,2,0)+\mathbf{g}_2$	3.08(8)	1.49	0.11	0.87
(0,2.8,1.2)	$(0,2,2)+\mathbf{g}_2'$	3.66(8)	2.33	0.07	1.60
(0,2.8,2.8)	$(0,2,2)+\mathbf{g}_2$	0.11(4)	0.02	0.11	0.18
(0,2.8,3.2)	$(0,2,4)+\mathbf{g}_2'$	0.06(4)	0.03	0.07	0.05
(0,3.2,0.8)	$(0,4,0)-\mathbf{g}_2'$	1.41(6)	1.85	0.07	1.20
(0,3.2,1.2)	$(0,4,2)-\mathbf{g}_2$	2.16(6)	2.72	0.11	1.86
(0,3.2,2.8)	$(0,4,2)-\mathbf{g}_2'$	0.16(4)	0.11	0.07	0.38
(0,3.2,3.2)	$(0,4,4)-\mathbf{g}_2$	0.15(4)	0.13	0.11	0.01

TABLE II. Parameter values obtained in fitting the observed values of $|F|^2$ for the $\mathbf{g}_2$ and $\mathbf{g}_1$ peaks.

$\mathbf{g}_2$ modulation		$\mathbf{g}_1$ modulation	
Parameter	Value	Parameter	Value
$\Delta y_{O_2} b$	0.153 Å	$\Delta x_{O_2} a$	0.120 Å
$\Delta y_{La} b$	−0.059 Å	$\Delta z_{O_2} c$	−0.121 Å
$\Delta z_{O_1,c} c$	−0.016 Å	$\Delta x_{La} a$	−0.082 Å
$\Delta z_{O_1,s} c$	−0.041 Å	$\Delta z_{La} c$	0.074 Å
		$\Delta y_{O_1} b$	0.028 Å

dominantly to the displacements of atoms in the original lattice, the small values require destructive interference between the contributions from the interstitials and the displacements. To illustrate this, we have also listed in Table I the values obtained from the model considering just the interstitial contribution, $|F_{\text{int}}|^2$, and just the displacement contribution, $|F_{\text{disp}}|^2$.

C. $\mathbf{g}_1$ structure

Applying the rigid-rotation model to the $\mathbf{g}_1$ modulation leads to the model shown on the left-hand side of Fig. 7. To model intensities of $(h0l)$ reflections, we consider only displacements of the apical O and the La. Besides a rotation-type displacement along **a**, we also allow a displacement perpendicular to the planes, with the pairs of O and of La associated with one NiO_2 layer moving in the same direction (i.e., not a breathing-type displacement). Figure 8 is an attempt to illustrate how the pattern of apical oxygen displacements is correlated with the positions of the interstitials. The density of interstitials per elementary unit cell in the **a-c** projection of Fig. 7 is $\frac{1}{3}$. Combining this value with the density of $\frac{4}{5}$ obtained for the **b-c** projection yields a net density of $\frac{4}{15}$ per unit cell. Since a unit cell contains two Ni atoms, the interstitial density corresponds to an oxygen excess per formula unit of $\delta = \frac{2}{15}$.

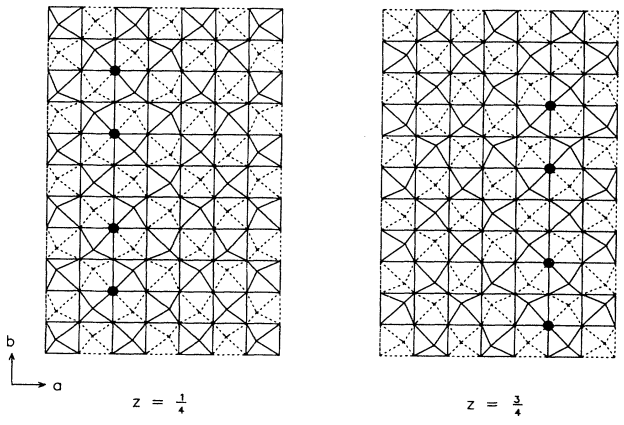

FIG. 8. Diagram indicating correlations between apical oxygen displacements and the locations of the interstitials at $z = \frac{1}{4}$ and at $z = \frac{3}{4}$. Lines indicate edges of NiO_6 octahedra. Solid lines denote tops of octahedra centered at $z - \frac{1}{4}$; dashed lines denote bottoms of octahedra centered at $z + \frac{1}{4}$. Interstitials sit in positions where all nearest-neighbor apical oxygens are tilted away.

The distortions associated with the two octahedra in the elemental unit cell are opposite to each other, so that the structure factor for the cell can be written in terms of the displacements for a single octahedron times the factor $1 - \exp[i\pi(k - l)]$, which is always equal to 2 for the observed $(h0l)$ and $(hk0)$ reflections. The relevant structure factors for the $(h0l)$ peaks are then

$$f_c = 8\pi h[b_O \Delta x_{O_2} \sin(2\pi l z_{O_2}) + b_{La} \Delta x_{La} \cos(\pi k) \sin(2\pi l z_{La})], \quad (24)$$

$$f_s = i8\pi l[b_O \Delta z_{O_2} \cos(2\pi l z_{O_2}) + b_{La} \Delta z_{La} \cos(\pi k) \cos(2\pi l z_{La})]. \quad (25)$$

(The contributions due directly to the interstitials are given in the Appendix.) Examination of these formulas reveals that they are equal to zero for $(hk0)$ reflections. To explain the intensity there, we consider displacements of the in-plane oxygens parallel to **b**, transverse to the modulation direction which is along **a**. The structure factor is

$$f_s = 8\pi k \Delta y_{O_1} e^{-i\frac{\pi}{2}h} \sin\left(\frac{\pi}{2}k\right), \quad (26)$$

with $f_c = 0$. In our model, there is no direct contribution from the intersitials to the $(hk0)$ intensities.

The observed values of $|F|^2$ are compared in Table III with those obtained from a least squares fit. The parameter values resulting from the fit are listed in Table II. Again, to illustrate the relative contributions and degree of interference, the values of $|F|^2$ calculated for (a) only the interstitial and (b) only the diplacement contributions are listed in the last two columns of Table III. The model seems to give adequate agreement with the observations.

V. ANALYSIS OF SPIN AND CHARGE ORDER

A. $\mathbf{g}_\epsilon$ structure

As mentioned earlier, the spin structure is characterized by the modulation wave vector

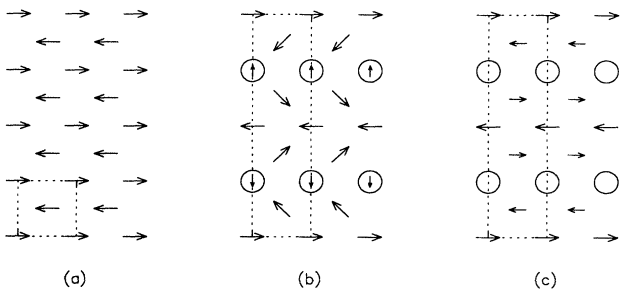

FIG. 9. (a) Undoped Néel structure, (b) spiral spin structure, (c) transverse collinear spin structure. Arrows indicate spins on Ni sites in an NiO_2 plane; circles denote expected positions of holes.

TABLE III. Comparison of the observed values of $|F|^2$ for the $\mathbf{g}_1$ peaks with those calculated using the model discussed in the text. Also included are the results calculated assuming that only the interstitials or only the displacements contribute.

(h,k,l)	$\mathbf{G} \pm \mathbf{g}_1$	$\lvert F\rvert^2_{\rm obs}$	$\lvert F\rvert^2_{\rm calc}$	$\lvert F_{\rm int}\rvert^2$	$\lvert F_{\rm disp}\rvert^2$
(0.33,0,1)	$(0,0,0)+\mathbf{g}_1$	0.04(1)	0.18	0.21	0.00
(0.33,0,3)	$(0,0,2)+\mathbf{g}_1$	0.16(1)	0.03	0.21	0.09
(0.33,0,5)	$(0,0,4)+\mathbf{g}_1$	0.26(2)	0.04	0.21	0.44
(0.33,0,7)	$(0,0,6)+\mathbf{g}_1$	0.25(3)	0.22	0.21	0.00
(1.67,0,1)	$(2,0,2)-\mathbf{g}_1$	0.05(2)	0.15	0.21	0.01
(1.67,0,3)	$(2,0,4)-\mathbf{g}_1$	0.21(2)	0.16	0.21	0.00
(1.67,0,7)	$(2,0,8)-\mathbf{g}_1$	1.61(6)	1.59	0.21	0.65
(2.33,0,5)	$(2,0,4)+\mathbf{g}_1$	1.22(6)	1.26	0.21	0.44
(3.67,0,1)	$(4,0,2)-\mathbf{g}_1$	0.31(4)	0.40	0.21	0.03
(0.67,1,0)	$(1,1,1)-\mathbf{g}_1$	0.05(4)	0.06	0.00	0.06
(1.33,1,0)	$(1,1,-1)+\mathbf{g}_1$	0.35(10)	0.06	0.00	0.06
(2.67,1,0)	$(3,1,1)-\mathbf{g}_1$	0.02(2)	0.06	0.00	0.06
(3.33,1,0)	$(3,1,-1)+\mathbf{g}_1$	0.08(4)	0.06	0.00	0.06
(0.67,3,0)	$(1,3,1)-\mathbf{g}_1$	0.27(8)	0.50	0.00	0.50
(1.33,3,0)	$(1,3,-1)+\mathbf{g}_1$	0.38(8)	0.50	0.00	0.50
(2.67,3,0)	$(3,3,1)-\mathbf{g}_1$	0.83(10)	0.50	0.00	0.50

$$\mathbf{g}_\epsilon = (1-\epsilon, 0, 0). \tag{27}$$

The fact that this is close to the antiferromagnetic wave vector (1,0,0) tells us that nearest-neighbor spins are approximately antiparallel, while the displacement by ϵ indicates that the magnitude and/or direction of spins must be modulated such that the repeat distance in real space lattice units is $1/\epsilon$. Since $\epsilon \approx \frac{1}{4}$, the period of the spin structure is approximately $4a$. Two possible structures are contrasted with the simple Néel structure in Fig. 9, where we have taken $\epsilon = \frac{1}{4}$ for simplicity. When the spins are collinear, as in Fig. 9(c), the magnetic moments are zero along stripes with a density of 1 out of 4 Ni sites. This density of sites is equal to the nominal hole density $p = 2\delta$ for $\delta = 0.125$, so it seems reasonable to associate the holes with the positions of minimum moment. Of course, while the antiparallel coupling of a hole spin with a Ni spin will lead to a reduced net moment, the moment will not be zero. Combining a spin-$\frac{1}{2}$ hole with a spin-1 Ni ion should yield a spin-$\frac{1}{2}$ object. A model with all spins finite can be obtained by adding a second spin component whose direction is perpendicular to, and whose modulation is $2\pi\epsilon$ out of phase with, the first component, as illustrated in Fig. 9(b).

To model the observed superlattice intensities, we begin with the general expression for the magnetic structure factor corresponding to the nth unit cell:

$$\mathbf{F}_{{\rm mag},n}(\mathbf{Q}) = \frac{r_0}{2\mu_B}\sum_{j,n}\mu_{j,n} f_j(\mathrm{Q})\mathbf{q}_j e^{-i\mathbf{Q}\cdot\mathbf{r}_j}, \tag{28}$$

where $r_0 = 0.539\times10^{-12}$ cm. The quantity $\mathbf{q}_j$ is related to the moment $\boldsymbol{\mu}_j$ by the formula

$$\mathbf{q}_j = \hat{\boldsymbol{\mu}}_j - (\hat{\mathbf{Q}}\cdot\hat{\boldsymbol{\mu}}_j)\hat{\mathbf{Q}}, \tag{29}$$

with a caret denoting a unit vector. Initially we will assume that all of the ordered spin density is on the Ni sites, so that $f_j(\mathbf{Q}) = f_{\rm Ni}(\mathbf{Q})$, the magnetic form factor for a Ni^{2+} ion. To consider general models of in-plane spin order, we consider separate moment components that are transverse ($\mu_\perp$) and longitudinal ($\mu_\parallel$) with respect to $\mathbf{g}_\epsilon$:

$$\mu_{\perp,n} = \mu_\perp \cos(\mathbf{g}_\epsilon\cdot\mathbf{R}_n), \tag{30}$$

$$\mu_{\parallel,n} = \mu_\parallel \cos(\mathbf{g}_\epsilon\cdot\mathbf{R}_n + \theta). \tag{31}$$

For finite $\mu_\perp$ and $\mu_\parallel$ with $\theta = 2\pi\epsilon$ we have the spiral structure; for $\theta = 0$ the net moments are collinear but diagonal; and with $\mu_\parallel = 0$ we get the transverse collinear structure. We can then make use of Eq. (14) to write the square of the structure factor for a single layer as

$$|F_{\rm mag}(\mathbf{Q})|^2 = \frac{1}{4}\left(\frac{r_0}{2\mu_B}\right)^2 f^2_{\rm Ni}(\mathbf{Q}) \times\left[\mu_\perp^2\left(1-\hat{Q}_y^2\right) - 2\mu_\perp\mu_\parallel\hat{Q}_x\hat{Q}_y\cos\theta + \mu_\parallel^2\left(1-\hat{Q}_x^2\right)\right]. \tag{32}$$

Since, for a given value of θ, there is no reason for $+\theta$ to be preferred over $-\theta$, we expect to have both types of domains present. Assuming that they occupy equal volumes of the crystal, averaging $|F|^2$ over the domains will cause the term proportional to $\cos\theta$ to average to zero. Thus, our measurements should not be sensitive to the relative phase of modulation of the $\mu_\perp$ and $\mu_\parallel$ components.

For $(h0l)$ reflections the intensities fluctuate only a small amount as a function of l, indicating that there is relatively little interference between the scattering contributions from the two layers per unit cell. It follows that the magnetic scattering amplitudes of neighboring layers must be approximately out of phase, so that in calculating the intensity the amplitudes from inequivalent layers combine incoherently. (We will return to this point below.) Hence to determine the relative magnitudes of $\mu_\perp$

and $\mu_{\|}$ we can analyze the intensities of $(hk0)$ peaks using the single layer structure factor given by Eq. (32), with the $\cos\theta$ term left out. In Fig. 10(a) we plot the values of $|F_{\rm mag}|^2$, divided by the square of the Ni form factor determined from La_2NiO_4,[20] for $(hk0)$ reflections as a function of $1-\hat{Q}_y^2$. The linear dependence indicated by the straight line is just what one expects for $\mu_{\|}=0$. Because $|F|^2$ depends on the sum of the squares of the two moment components, it is difficult to rule out a small but finite value for $\mu_{\|}$. A reasonable limit is $\mu_{\|}/\mu_{\perp}<0.2$. For the rest of the analysis we will assume $\mu_{\|}=0$.

We have now identified the general features of the low-temperature spin structure in $La_2NiO_{4.125}$: (1) the sinusoidally modulated Ni spins within a plane point transversely with respect to $\mathbf{g}_{\epsilon}$, and (2) the modulations in neighboring planes differ in phase by approximately $\pi/2$. Using this model, we can invert Eq. (32) to obtain $\mu_{\perp}f(Q)$ from the observed values of $|F_{\rm mag}|^2$. One would expect $f_{\rm Ni}(Q)$ to vary reasonably smoothly with Q; however, the experimentally obtained results show a degree of scatter that is significantly larger than one might expect based on the experimental uncertainties. We have found that the scatter can be reduced somewhat by including some refinements in the model. The first refinement is to allow the modulation phase difference between neighboring planes to differ from $\pi/2$ by a small amount α. The other revision is to allow for spin density on the apical oxygen and lanthanum ions. Net spin densities on these ions may be expected due to hybridization with the half-filled Ni $3d_{3z^2-r^2}$ orbital. Evidence for spin density on La ions in doped La_2NiO_4 has been found in two previous studies,[21,22] and any moment on La should involve hybridization through the apical oxygen. Following Lander *et al.*[21] we assume that the form factor for La can be approximated by $f_{\rm Ni}$. For oxygen we use

$$f'_{\rm O}=f_{\rm O}/f_{\rm Ni}=e^{-Q^2/2\sigma_{\rm O}^2}, \tag{33}$$

where the width parameter $\sigma_{\rm O}$ is somewhat arbitrarily chosen to be 2.4 Å^{-1}, approximately half of the width required to describe $f_{\rm Ni}$. (The analysis is fairly insensitive to the precise value of $\sigma_{\rm O}$.) If we first define

$$\mathcal{F}=\mu_{\perp}f_{\rm Ni}(1+2\beta_{\rm O2}f'_{\rm O}\cos 2\pi z_{\rm O_2}l + 2\beta_{\rm La}\cos 2\pi z_{\rm La}l), \tag{34}$$

then we can express the refined model as

$$|F_{\rm mag}|^2=\frac{1}{2}\left(\frac{r_0}{2\mu_B}\right)^2\mathcal{F}^2 \times[1+|\sin\alpha|\cos\pi(k+l)](1-\hat{Q}_y^2). \tag{35}$$

To fit this model to the measured values of $|F_{\rm mag}|^2$ we set

$$\mu_{\perp}f_{\rm Ni}=\mu_0 e^{-Q^2/2\sigma_{\rm Ni}^2}, \tag{36}$$

with μ_0 and $\sigma_{\rm Ni}$ treated as fitting variables. The parameter values obtained from the fitting are $\alpha=0.08$ rad, $\beta_{\rm O2}=0.041$, and $\beta_{\rm La}=0.008$. We then solved Eqs. (34) and (35) for $\mu_{\perp}f_{\rm Ni}$ and calculated values from the measured $|F_{\rm mag}|^2$ using the fitted values of α, $\beta_{\rm O_2}$, and $\beta_{\rm La}$. The results are shown in Fig. 10(b), where they are compared with the values of $\mu f_{\rm Ni}$ obtained in undoped La_2NiO_4 by Wang *et al.*[20] As one can see from the figure, the amplitude of the moment modulation in the $\delta=0.125$ compound is more than 80% of the moment found in the undoped material.

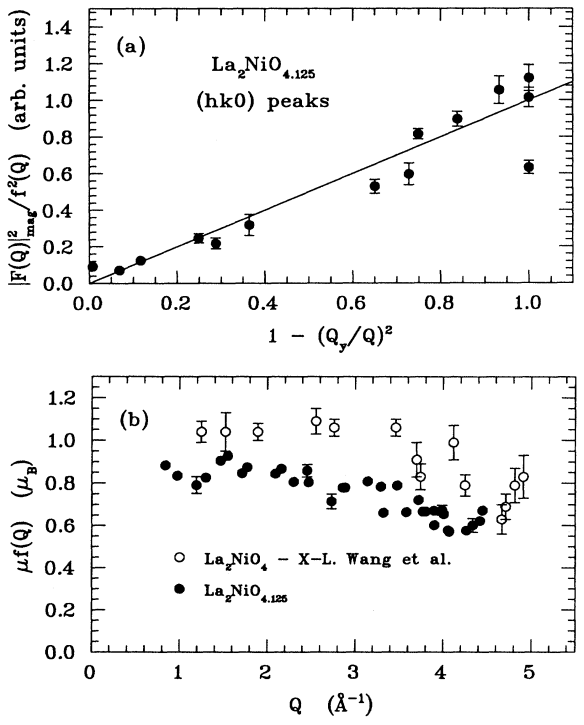

FIG. 10. (a) Plot of observed values of $|F|^2$, divided by the square of the Ni magnetic form factor, for magnetic superlattice peaks in the $(hk0)$ zone plotted vs $1-\hat{Q}_y^2$. The solid line indicates the behavior expected if all spins are parallel to the b axis. (b) Values of the ordered magnetic moment μ times the magnetic form factor f as a function of Q in $La_2NiO_{4+\delta}$ extracted for $\delta=0.125$ (solid circles), $\delta=0$ (open circles). The $\delta=0$ results are from the work of Wang *et al.* (Ref. 20).

B. $\mathbf{g}_{2\epsilon}$ structure

In our earlier report[12] we associated the $\mathbf{g}_{2\epsilon}$ peaks with a charge-density-wave distortion corresponding to periodically ordered stripes of holes. Neutrons, of course, do not scatter directly from the charge density; instead, they can be diffracted by the atomic displacement waves that will be induced if there is a charge modulation that differs from the nuclear periodicity. To "prove" that the $\mathbf{g}_{2\epsilon}$ peaks do indeed indicate a charge-density modulation, we must show that the peak intensities are generated by an atomic displacement pattern that corresponds to an appropriate modulation of bond lengths.

Zaanen and Littlewood[13] have recently published the results of Hartree-Fock calculations on a three-band Hubbard model (including Peierls-type electron-phonon cou-

pling) using parameter values appropriate for a doped NiO_2 plane. Their calculations indicate that the holes tend to form "diagonal" domain walls centered on rows of Ni atoms, with a substantial reduction of the Ni-O bond length ($\sim 5\%$) in the region of maximum hole density. The charge density and bond deformation patterns are not identical, and we will return to this point later.

As a starting model for analyzing the superlattice intensities, we assumed naively that the Ni-O bonds along the [100] direction in a NiO_2 layer should have a simple sinusoidal modulation. The corresponding displacement pattern for Ni and O ions is indicated in Fig. 11. The pair of apical oxygens about a Ni site is assumed to move identically with the Ni, while the La ions are allowed to move parallel to the a axis with an arbitrary displacement. In terms of the partial structure factors f_s and f_c, the model can be expressed as

$$f_s = -i4\pi\Big\{h\Delta x_{\mathrm{Ni}}[b_{\mathrm{Ni}} + 2b_{\mathrm{O}}\cos(2\pi z_{\mathrm{O}_2} l)] + 2\Delta r_{\mathrm{O}_1} b_{\mathrm{O}} e^{-i\pi h/2}\cos\theta + 2h\Delta x_{\mathrm{La}} b_{\mathrm{La}}\cos\pi k\cos(2\pi z'_{\mathrm{La}} l)\Big\}, \quad (37)$$

$$f_c = -i4\pi\Big\{2\Delta r_{\mathrm{O}_1} b_{\mathrm{O}} e^{-i\pi h/2}\sin\theta\Big\}, \quad (38)$$

where $z'_{\mathrm{La}} = \frac{1}{2} - z_{\mathrm{La}}$,

$$\Delta r_{\mathrm{O}_1} = h\Delta x_{\mathrm{O}_1}\cos(\pi k/2) + k\Delta y_{\mathrm{O}_1}\sin(\pi k/2) \quad (39)$$

and where, for a simple sinusoidal bond-length modulation, we must fix $\Delta x_{\mathrm{Ni}} = \Delta x_{\mathrm{O}_1}$ and $\theta = \pi\epsilon$.

The values of $|F|^2$ calculated with this model (labeled model 1) are compared with the observed values in Table IV; the parameter values obtained from the fit are listed in Table V. The quality of the fit is not very satisfactory. To get an improved fit, we have allowed the *phase* of the displacement modulation for the in-plane oxygens to differ from that for the Ni and La (i.e., θ is allowed to vary), and the displacement *amplitude* for Ni is allowed to be independent of that for O_1. The results obtained from fitting the latter model (see model 2 in Tables IV and V) are clearly in much better agreement with the data. A graphical comparison of the observed and fitted $|F|^2$ values is given in Fig. 12.

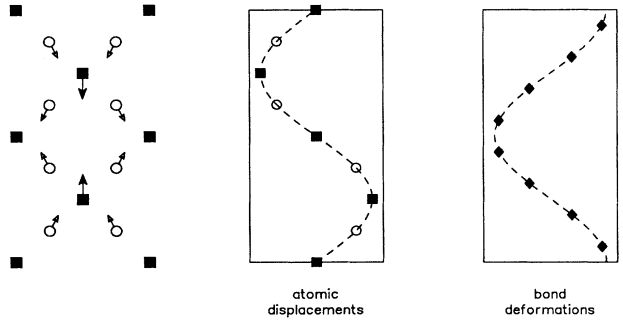

FIG. 11. Sketch of the expected atomic displacements and bond deformations associated with the charge-density-wave order. Squares, Ni; circles, O; diamonds, bond deformations.

The Ni-O bond deformation patterns calculated from models 1 and 2, using the parameter values in Table V, are presented in Fig. 13. For model 1, $\Delta d/d$ shows the simple sinusoidal modulation with period $1/2\epsilon$ that was built into the model; the peak-to-peak amplitude is 0.8%. For model 2, the bond displacement pattern appears much less regular. The underlying periodicity becomes

TABLE IV. Comparison of the observed values of $|F|^2$ for the $\mathbf{g}_{2\epsilon}$ peaks with those calculated using the models discussed in the text. The values of χ^2 obtained for the two models are given at the bottom.

(h,k,l)	$\mathbf{G} \pm \mathbf{g}_{2\epsilon}$	$\lvert F\rvert^2_{\mathrm{obs}}$	$\lvert F\rvert^2_{\mathrm{calc}}$	
			Model 1	Model 2
(0.45,1,0)	$(1,1,1) - \mathbf{g}_{2\epsilon}$	0.00(1)	0.02	0.02
(1.55,1,0)	$(1,1,-1) + \mathbf{g}_{2\epsilon}$	0.04(1)	0.08	0.09
(2.45,1,0)	$(3,1,1) - \mathbf{g}_{2\epsilon}$	0.41(3)	0.23	0.24
(3.55,1,0)	$(3,1,-1) + \mathbf{g}_{2\epsilon}$	0.64(3)	0.65	0.65
(0.45,3,0)	$(1,3,1) - \mathbf{g}_{2\epsilon}$	0.08(2)	0.00	0.04
(1.55,3,0)	$(1,3,-1) + \mathbf{g}_{2\epsilon}$	0.21(3)	0.22	0.24
(0.55,0,1)	$(0,0,0) + \mathbf{g}_{2\epsilon}$	0.01(1)	0.01	0.02
(0.55,0,3)	$(0,0,2) + \mathbf{g}_{2\epsilon}$	0.01(1)	0.00	0.01
(0.55,0,5)	$(0,0,4) + \mathbf{g}_{2\epsilon}$	0.14(1)	0.01	0.02
(0.55,0,7)	$(0,0,6) + \mathbf{g}_{2\epsilon}$	0.04(3)	0.01	0.02
(1.45,0,1)	$(2,0,2) - \mathbf{g}_{2\epsilon}$	0.00(1)	0.08	0.02
(1.45,0,3)	$(2,0,4) - \mathbf{g}_{2\epsilon}$	0.02(1)	0.02	0.03
(1.45,0,5)	$(2,0,6) - \mathbf{g}_{2\epsilon}$	0.06(4)	0.06	0.02
(1.45,0,7)	$(2,0,8) - \mathbf{g}_{2\epsilon}$	0.00(2)	0.10	0.02
(2.55,0,1)	$(2,0,0) + \mathbf{g}_{2\epsilon}$	0.07(2)	0.25	0.05
(2.55,0,3)	$(2,0,2) + \mathbf{g}_{2\epsilon}$	0.02(2)	0.08	0.10
(2.55,0,5)	$(2,0,4) + \mathbf{g}_{2\epsilon}$	0.13(2)	0.20	0.05
(3.45,0,1)	$(4,0,2) - \mathbf{g}_{2\epsilon}$	0.72(3)	0.35	0.70
(3.45,0,3)	$(4,0,4) - \mathbf{g}_{2\epsilon}$	0.42(2)	0.14	0.43
χ^2			7.0	4.3

TABLE V. Parameter values obtained in fitting models 1 and 2 to the observed values of $|F|^2$ for the $\mathbf{g}_{2\epsilon}$ peaks.

Parameter	Model 1	Model 2
$\Delta x_{O_1} a$	0.013 Å	0.018 Å
$\Delta y_{O_1} b$	0.005 Å	0.009 Å
$\Delta x_{Ni} a$	$\Delta x_{O_1} a$	0.010 Å
$\Delta x_{La} a$	−0.001 Å	−0.004 Å
θ	$\pi\epsilon$	−0.322 rad

clear only when one looks at every second bond, as indicated by the dashed lines in the figure. This pattern results from the phase shift between the modulations of the Ni and O displacements.

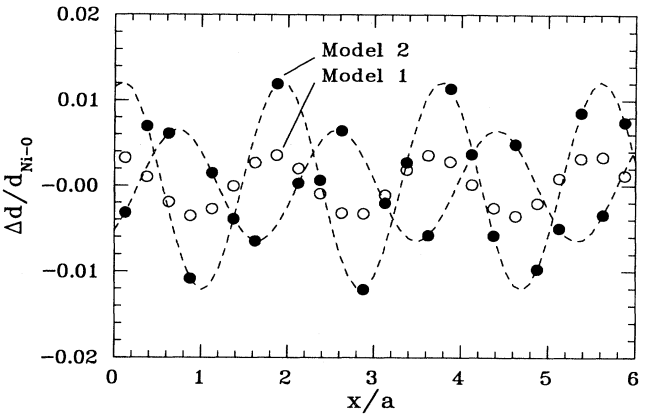

FIG. 13. Relative bond length variations vs positions along the a axis for the two models discussed in the text.

VI. DISCUSSION

A. Nature of the spin and charge order

We have shown that the superlattice peaks which appear in $La_2NiO_{4.125}$ below 110 K are consistent with a cooperative ordering of spins and holes of the type shown in Fig. 9(c). Both the spin and charge densities are sinusoidally modulated, with the spins oriented perpendicular to the modulation direction. (The modulation of the charge density is inferred from the directly observed atomic displacements.) Although we have no direct measure of the relative phases, we expect that the maximum of the hole density modulation coincides with the minimum of the spin-density wave. The maximum magnetic moment per Ni site is quite close to the value observed[20] in undoped La_2NiO_4. The large amplitude of the spin-density modulation, together with the substantial dopant-induced hole concentration, implies a very strong modulation of the hole density.

It is difficult to quote an absolute magnitude because of discrepancies between experimental and theoretical magnetic form factors.[20] A recent theoretical study[23] of the

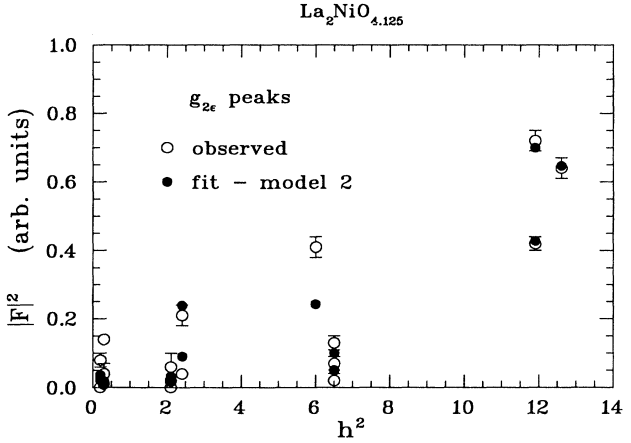

FIG. 12. Values of $|F|^2$ for $\mathbf{g}_{2\epsilon}$ peaks vs h^2. Open circles, observed values; filled circles, values calculated with model 2 (discussed in text).

Ni^{2+} form factor found reasonable agreement between calculations and measurements for $KNiF_3$ and NiO; however, the form factor measured[20] for La_2NiO_4 falls significantly below the calculated one at small Q. The form factor we find for the $\delta = 0.125$ sample agrees well with that measured for $\delta = 0$ (see Fig. 10). The discrepancy with theory remains to be resolved.

We note that our experimental observations are completely consistent with those of Yamada *et al.*,[15] who were the first to observe the incommensurate magnetic order; however, our model for the order is somewhat different. The spin model shown in Fig. 6 of Ref. 15 has the correct overall period, but is locally ferromagnetic rather than antiferromagnetic. Thus, it corresponds to a modulation wave vector of $(\epsilon, 0, 0)$, rather than the observed $(1-\epsilon, 0, 0)$. Also, their proposal for ordering of the holes is not consistent with our observation of second harmonic peaks.

The fact that the spin and charge modulations are sinusoidal was a surprise to us; however, this conclusion is an inescapable consequence of the observations. Deviations of the spin modulation from a pure sine wave will induce higher-order odd harmonics; indeed, we do observe a very weak third-harmonic peak indicating a small distortion of the spin-density wave. No even harmonics beyond the second have been observed.

The role of the interstitial ordering with respect to the spin and charge order is not yet clear. The change from commensurate to incommensurate magnetic order, which occurs between $\delta = 0.105$ and 0.116, is correlated with a change in the interstitial correlations, from 1D staging to 3D order.[12] In both cases the magnetic order is long range, but hole ordering has only been detected in the latter case. To further investigate the change in behavior, a study of the dynamical correlations in the paramagnetic state of the $\delta = 0.105$ and $\delta = 0.125$ crystals is under way.

B. Comparison with theory

In discussing possible models of spin and charge order, it was convenient to consider a hole density of one per

four Ni atoms, consistent with the oxygen excess of $\delta = 0.125$ with two holes created per oxygen. Experimentally the ideal splitting, $\epsilon = \frac{1}{4}$, is not observed; instead, the temperature-dependent splitting reaches a minimum of 0.271 at low temperature.[12,15] As discussed previously,[12] it appears that, instead of being incommensurate, the order is actually long-period commensurate. Below 60 K the dominant ordering corresponds to $\epsilon = \frac{3}{11}$. To make comparisons with theory it is useful to plot the spin and charge densities for this case.

Figure 14 shows such a plot, with holes assumed to be on the oxygens. The phase of the spin modulation with respect to the lattice has been selected arbitrarily. The hole density has been drawn with some artistic license. In the previous section we saw that the bond-length modulation follows a somewhat complicated pattern, and its relation to the charge distribution is not entirely obvious. As a result, we have simply assumed that the charge modulation is a simple sine wave that has its maximum amplitude where the spin density is a minimum.

Our results look qualitatively quite similar to the calculations of Zaanen and Littlewood.[13] They find that the hole-rich domain walls tend to be centered on Ni rows; however, their charge distribution is asymmetric, and the bond lengths do not have a simple, smooth variation. Figure 14 indicates that, experimentally, there is a mixture of domain walls centered both on Ni rows and on O rows. We also observe a tendency to have a ferromagnetic alignment of the reduced Ni spins at a domain wall, consistent with the calculations.[13] Perhaps the biggest discrepancy concerns the width of the domain walls relative to the antiferromagnetic background. The calculations yield sharp domain walls relative to their spacing (although details are dependent on parameter values), in contrast to the experimentally observed sinusoidal modulation of the spin and charge densities. Variational Monte Carlo analyses[10,11] of the 2D single-band Hubbard model indicate that narrow domain walls are an artifact of the Hartree-Fock approximation. Broader domain walls help to minimize the kinetic energy of the holes, although at a cost in terms of the potential energy associated with the antiferromagnetic spin order.

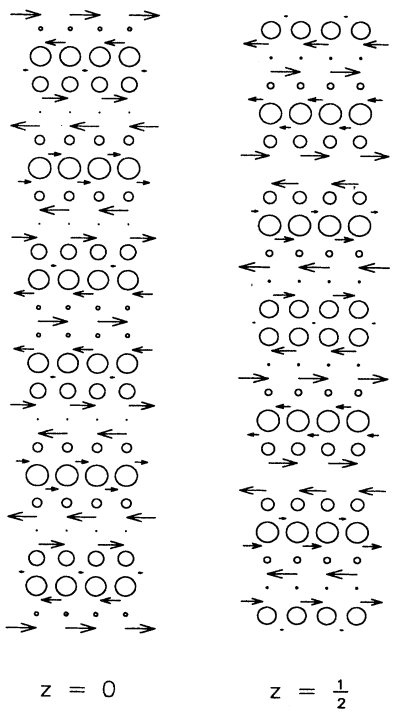

FIG. 14. Pattern of spin density (on Ni ions, indicated by arrows) and speculative charge density (on O ions, indicated by circles) in two neighboring NiO_2 planes for $\epsilon = \frac{3}{11}$.

The idea that the spin and charge stripes prefer a long-period commensurate order is based on the observed[12] tendency for ϵ to lock in to values that can be expressed as rational fractions of the form $(n+m)/(4n+3m)$. Examination of the unit cell shown in Fig. 14 suggests an explanation for this particular formula. For $\epsilon = \frac{3}{11}$, which corresponds to $n = 2$ and $m = 1$, we find for the $z = 0$ layer that there are $2n$ $(= 4)$ domain walls centered (approximately) on rows of Ni atoms and $2m$ $(= 2)$ domain walls centered on O rows. The pattern is approximately reversed for the $z = \frac{1}{2}$ layer, with $2n$ O-centered and $2m$ Ni-centered domain walls.

The theoretical explanation[13] for the insulating behavior follows from the 1D nature of the ordering. With one hole per domain wall unit cell, a Peierls distortion can open a gap in the conduction band, resulting in a finite excitation energy for conduction. The nominal hole concentration and domain wall periodicity in our $\delta = 0.125$ sample are very close to this condition. Of course, the fact that all domain walls are not equivalent will have some effect on the electronic structure. Is it possible that the observed periodicity and its temperature dependence are related to the energy gain from opening a gap at the Fermi level?

C. Comparison with $La_{2-x}Sr_xNiO_4$

We have shown[24] recently that a similar cooperative ordering of holes and spins occurs in $La_{2-x}Sr_xNiO_4$. For the samples studied ($x = 0.135$ and 0.20) the order is only short-ranged, especially between different NiO_2 planes. On the other hand, the incommensurate order evolves more smoothly with hole concentration than in the oxygen-doped case. The Sr-doped samples make it clear that 3D order of the dopant ions is not required to generate the 2D incommensurate order. Our model of charge and spin order has some similarity to the antiphase-domain picture originally developed by Brown *et al.*[25] to explain the first observation of incommensurate magnetic correlations in $La_{1.8}Sr_{0.2}NiO_{4-\delta}$ by Hayden *et al.*[26]

At higher Sr-doping levels, Cheong and co-workers[27,28] have found evidence for charge-ordered states corresponding to hole concentrations of $\frac{1}{3}$ and $\frac{1}{2}$. Electron diffraction measurements show superlattice peaks that, using our notation, can be described by a modulation wave vector $\mathbf{g}_{2\epsilon}$ with $\epsilon = \frac{1}{3}$ and $\frac{1}{2}$, respectively. Chen *et al.*,[27] using a different choice of modulation wave vector,

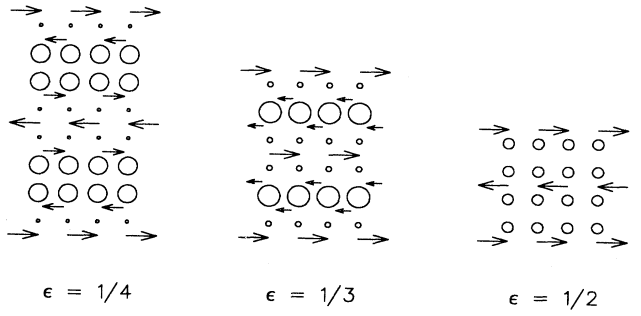

FIG. 15. Proposed progression of spin and charge modulations in NiO_2 planes with increasing hole concentration.

interpreted the diffraction results in terms of the ordering of polarons. For $\epsilon = \frac{1}{2}$ the polaron lattice description is essentially the same as the ordered domain wall picture—a row of Ni-centered polarons is equivalent to a domain wall; however, at $\epsilon = \frac{1}{3}$ the two descriptions are distinct. Chen *et al.*[27] propose a structure in which the rows of polarons are broken up by periodically spaced defects (polaron vacancies). Such an ordering is appropriate if one requires the holes to be centered about Ni sites. On the other hand, our results for $La_2NiO_{4.125}$ indicate that holes can be centered on O rows as well, and such an ordering makes it possible to maintain the domain wall description at $\epsilon = \frac{1}{3}$, as illustrated in Fig. 15. (Note that the corresponding spacing of the domain walls is $\frac{3}{2}a$. Zaanen and Littlewood[13] suggested a model in which every third domain wall is removed from the $x = \frac{1}{2}$ lattice. Such a structure has the same domain wall density as our model, but is extremely nonsinusoidal. It would result in strong higher harmonics, which have not been reported.[27]) A neutron diffraction study of both the spin and charge ordering at $x = \frac{1}{3}$ would help to resolve this situation.

D. Possible relevance to $La_{2-x}Sr_xCuO_4$

Neutron scattering studies[29–31] have revealed incommensurate peaks in the dynamical spin susceptibility of $La_{2-x}Sr_xCuO_4$. As in the nickelate case, four peaks are observed, split about the antiferromagnetic wave vector, but rotated by 45° compared to the nickelates. The "standard" interpretation of these features has been in terms of the response of electrons near the Fermi level, with the **Q** dependence determined by the shape of the Fermi surface.[32–34] Another probe of the spin susceptibility is nuclear magnetic resonance (NMR). The Mila-Rice-Shastry model[35,36] implies a simple connection between the nuclear relaxation rates measured at Cu and O sites, on the one hand, and the susceptibility measured directly by neutron scattering on the other. However, recent comparisons of the neutron and NMR results have found that the straightforward analysis leads to substantial inconsistencies.[37,38]

One proposal[38] for reconciling the neutron and NMR results involves the invocation of an ordering of the charge in domain walls. In such an interpretation, the facts that the inelastic magnetic peaks measured by neutron scattering are split away from the antiferromagnetic wave vector and have a relatively small Q width imply that the domain walls must be periodically spaced, with a substantial correlation length. The lack of higher harmonics indicates a sinusoidal modulation of the spin density. The required correlations are just the same as those we have found in the nickelates, except for two differences: the domain walls are rotated by 45° with respect to the simple square lattice (i.e., vertical, rather than diagonal, domain walls), and the correlations are purely dynamical. It will be interesting to see whether proper calculations based on such a model can give a consistent and unified interpretation of the experimental results.

Of course, if a correlated phase of charge and spin stripes exists in $La_{2-x}Sr_xCuO_4$, the implications for models of the normal state electronic properties are more than a minor perturbation. Indeed, Emery and Kivelson[2] have argued that such correlations are responsible for many of the anomalous normal state transport properties observed in the superconducting cuprates. One obvious objection to comparing the cuprates to the nickelates is that the cuprates are metallic while the nickelates are not; however, the insulating behavior of the ordered domain wall phase in the nickelates is presumably associated with half-filled domain wall states. A deviation from this filling fraction should lead to metallic behavior. In fact, an estimate for $La_{1.85}Sr_{0.15}CuO_4$, based on the positions of the incommensurate peaks observed by neutron scattering,[29–31] suggests that the hole density per domain wall should be roughly half that in the nickelates. Thus, a correlated domain wall phase should not be inconsistent with metallic behavior.

The correlated domain wall phase also gives a possible explanation for another mystery. The superconducting transition temperature in $La_{2-x}Ba_xCuO_4$ shows an anomalous depression at $x = 0.125$.[39] A phase transition from the low-temperature-orthorhombic to the low-temperature-tetragonal phase has a nonunique association with the disappearance of superconductivity and loss of metallic conductivity.[40] If at $x = 0.125$ the domain walls were to lock into a commensurate periodicity, the change in transport properties might be explained. If the commensurability energy caused a change in the domain wall hole concentration to one hole per site, an energy gap could open, resulting in insulating behavior. On the other hand, simply pinning the domain walls might be sufficient to eliminate the superconductivity. In either case, the commensurate pinning should result in the appearance of both spin- and charge-related superlattice peaks. An experimental search for such order will be reported elsewhere.[41]

VII. SUMMARY

We have presented a comprehensive quantitative analysis of the superlattice peaks that appear at low temperature in $La_2NiO_{4.125}$. The ordering of oxygen intersti-

tials below ~ 310 K is characterized by wave vectors $\mathbf{g}_1$ and $\mathbf{g}_2$. The interstitials arrange themselves in a somewhat complicated pattern that requires a unit cell of $3\mathbf{a} \times 5\mathbf{b} \times 5\mathbf{c}$ and corresponds to an ideal oxygen excess of $\delta = \frac{2}{15}$ per formula unit. Most of the scattered intensity comes from the displacements of apical O and La atoms in the lattice.

The ordering of spins and charges below 110 K is characterized by wave vectors $\mathbf{g}_\epsilon$ and $\mathbf{g}_{2\epsilon}$, respectively. The ordering involves sinusoidal modulations of the spin density and the Ni-O bond lengths within the NiO_2 planes. It can be viewed as alternating stripes of antiferromagnetic and hole-rich regions, with the hole-rich regions acting as antiphase-domain boundaries. The positions of the domain walls are staggered in neighboring layers as one would expect due to Coulomb repulsion. The maximum magnetic moment per Ni ion is close to that in undoped La_2NiO_4, and the spins point transverse to the modulation direction.

The observed spin and bond-length correlations are quite similar to the results of calculations by Zaanen and Littlewood[13] using a multiband Hubbard model with parameters appropriate to a NiO_2 plane. The physical realization of such a stripe phase provides further motivation for considering the applicability of such correlations to the cuprates.[2] On the experimental side, it will be interesting to see whether unique evidence can be found for domain wall correlations in the cuprates.

ACKNOWLEDGMENTS

We gratefully acknowledge valuable discussions with V. J. Emery and J. Zaanen, and we thank J. D. Axe for a critical reading of the manuscript. Work at Brookhaven was carried out under Contract No. DE-AC02-76CH00016, Division of Materials Sciences, U.S. Department of Energy. D.J.B. and V.S. acknowledge support from the National Science Foundation under Contract No. DMR-8914080.

APPENDIX: STRUCTURE FACTOR FOR THE ORDERED INTERSTITIALS

To describe the structure factor corresponding to atomic displacements we have expressed the displacements in the nth elemental unit cell in terms of the factors $\cos(\mathbf{g}_j \cdot \mathbf{R}_n)$ and $\sin(\mathbf{g}_j \cdot \mathbf{R}_n)$. We wish to include the contributions due to scattering directly from the interstitials in a similar form. Since not all elemental unit cells contain an interstitial, we can write the structure factor for the interstitial in the nth cell as

$$F_n = F_i \delta_{ni}, \tag{A1}$$

where i labels those cells that actually contain an interstitial. The problem is then to write δ_{ni} in terms of factors such as $\cos(\mathbf{g}_j \cdot \mathbf{R}_n)$.

Let $\mathbf{R}_n = (x_n a, y_n b, z_n c)$; then, considering the periodicity of the interstitial ordering, it is convenient to define the relative coordinates

$$\begin{aligned} x'_n &= x_n \bmod 3, \\ y'_n &= y_n \bmod 5, \\ z'_n &= z_n \bmod 5. \end{aligned}$$

Since we have distinct orderings along the x and y directions, corresponding to $\mathbf{g}_1$ and $\mathbf{g}_2$, we must write δ_{ni} as the product of two Kronecker deltas, so that

$$F_n = \sum_{s,t} F_{s,t} \delta_{x'_n,s} \delta_{y'_n+z'_n,t}, \tag{A2}$$

where the indices s and t can each have the values $+1$ and -1. For our model of the interstitial order we require

$$\delta_{x'_n,\pm 1} = \begin{cases} 1 & \text{if } x'_n = \pm 1, \\ 0 & \text{otherwise,} \end{cases} \tag{A3}$$

$$\delta_{y'_n+z'_n,\pm 1} = \begin{cases} 1 & \text{if } y'_n + z'_n = \pm 1, \mp 1.5, \\ 0 & \text{otherwise,} \end{cases} \tag{A4}$$

and

$$F_{\pm 1,+1} = e^{i\pi(k-l)} e^{\pm i \frac{\pi}{2}(h-k+l)}, \tag{A5}$$

$$F_{\pm 1,-1} = e^{-i\pi l} e^{\pm i \frac{\pi}{2}(h-k+l)}. \tag{A6}$$

The Kronecker deltas can be written as

$$\begin{aligned} \delta_{x'_n,\pm 1} = \frac{1}{3} \Big\{ \frac{1}{2} \Big[1 - \cos 3 \Big(\mathbf{g}_1 \cdot \mathbf{R}_n \mp \frac{\pi}{3} \Big) \Big] \\ - \cos \Big(\mathbf{g}_1 \cdot \mathbf{R}_n \mp \frac{\pi}{3} \Big) \\ + \cos 2 \Big(\mathbf{g}_1 \cdot \mathbf{R}_n \mp \frac{\pi}{3} \Big) \Big\} \end{aligned} \tag{A7}$$

and

$$\begin{aligned} \delta_{y'_n+z'_n,\pm 1} = \frac{1}{5} \Big[1 + 2 \cos \Big(\mathbf{g}_2 \cdot \mathbf{R}_n \pm \frac{2\pi}{5} \Big) \\ + 2 \cos 2 \Big(\mathbf{g}_2 \cdot \mathbf{R}_n \pm \frac{2\pi}{5} \Big) \Big]. \end{aligned} \tag{A8}$$

If we consider $\mathbf{g}'_2$ instead of $\mathbf{g}_2$, there are some sign changes that we will take into account below.

To determine the contributions to different diffraction peaks, we multiply out factors in Eq. (A2), and collect terms proportional to $\cos m(\mathbf{g}_j \cdot \mathbf{R}_n)$ and to $\sin m(\mathbf{g}_j \cdot \mathbf{R}_n)$. (Cross terms average to zero when the intensity is calculated properly, and so are of no consequence.) Terms corresponding to $m = 0$ (and $m = 3$ for $j = 1$) contribute to the fundamental Bragg peaks; they are negligible compared to the scattering from the lattice, and so have been ignored. The $m = 2$ terms determine the intensities of the second harmonic peaks, which we have not studied with any care. Here we consider just the first harmonic $m = 1$ terms. We can define partial structure factors f_c and f_s for each of the modulation wave vectors by analogy with Eq. (11). To simplify the expressions, we first define

$$f_I = \frac{2}{15} e^{-i\pi(\eta k+l)\cos\frac{\pi}{2}(h+\eta k+l)}, \tag{A9}$$

where

$$\eta = \begin{cases} +1 & \text{for } \mathbf{g}_1 \text{ and } \mathbf{g}_2', \\ -1 & \text{for } \mathbf{g}_2. \end{cases} \tag{A10}$$

We then find for $\mathbf{g}_1$

$$f_c = -f_I(1+e^{i\pi k})\cos\frac{\pi}{3}, \tag{A11}$$

$$f_s = -if_I(1+e^{i\pi k})\sin\frac{\pi}{3}, \tag{A12}$$

and for $\mathbf{g}_2$ and $\mathbf{g}_2'$

$$f_c = f_I(1+\cos\pi k + i\eta\sin\pi k)\cos\frac{2\pi}{5}, \tag{A13}$$

$$f_s = f_I[\eta(1-\cos\pi k) - i\sin\pi k]\sin\frac{2\pi}{5}. \tag{A14}$$

* Present address: European Synchrotron Radiation Facility, B.P. 220, F-38043 Grenoble Cedex, France.

[1] V. J. Emery and S. A. Kivelson, Physica C **209**, 597 (1993).
[2] V. J. Emery and S. A. Kivelson, Physica C **235-240**, 189 (1994).
[3] S. A. Kivelson and V. J. Emery, in *Strongly Correlated Electronic Materials: The Los Alamos Symposium 1993*, edited by K. S. Bedell *et al.* (Addison-Wesley, Reading, MA, 1994), pp. 619–656.
[4] D. Poilblanc and T. M. Rice, Phys. Rev. B **39**, 9749 (1989).
[5] J. Zaanen and O. Gunnarsson, Phys. Rev. B **40**, 7391 (1989).
[6] H. J. Schulz, Phys. Rev. Lett. **64**, 1445 (1990).
[7] M. Kato, K. Machida, H. Nakanishi, and M. Fujita, J. Phys. Soc. Jpn. **59**, 1047 (1990).
[8] J. A. Vergés *et al.*, Phys. Rev. B **43**, 6099 (1991).
[9] M. Inui and P. B. Littlewood, Phys. Rev. B **44**, 4415 (1991).
[10] T. Giamarchi and C. Lhuillier, Phys. Rev. B **42**, 10641 (1990).
[11] G. An and J. M. J. van Leeuwen, Phys. Rev. B **44**, 9410 (1991).
[12] J. M. Tranquada, D. J. Buttrey, V. Sachan, and J. E. Lorenzo, Phys. Rev. Lett. **73**, 1003 (1994).
[13] J. Zaanen and P. B. Littlewood, Phys. Rev. B **50**, 7222 (1994).
[14] D. E. Rice and D. J. Buttrey, J. Solid State Chem. **105**, 197 (1993).
[15] K. Yamada *et al.*, Physica C **221**, 355 (1994).
[16] J. M. Tranquada *et al.*, Phys. Rev. B **50**, 6340 (1994).
[17] J. E. Lorenzo, J. M. Tranquada, D. J. Buttrey, and V. Sachan, Phys. Rev. B **51**, 3176 (1995).
[18] R. P. Scaringe and R. Comés, in *Physical Methods of Chemistry*, edited by B. W. Rossiter and J. F. Hamilton (John Wiley & Sons, New York, 1990), pp. 517–601.
[19] J. M. Tranquada, D. J. Buttrey, and D. E. Rice, Phys. Rev. Lett. **70**, 445 (1993).
[20] X.-L. Wang *et al.*, Phys. Rev. B **45**, 5645 (1992).
[21] G. H. Lander *et al.*, Phys. Rev. B **43**, 448 (1991).
[22] S. Wada *et al.*, J. Phys. Condens. Matter **5**, 765 (1993).
[23] H. Chang, J. F. Harrison, T. A. Kaplan, and S. D. Mahanti, Phys. Rev. B **49**, 15753 (1994).
[24] V. Sachan *et al.*, Phys. Rev. B **51**, 12 742 (1995).
[25] P. J. Brown *et al.*, Physica B **180 & 181**, 380 (1992).
[26] S. M. Hayden *et al.*, Phys. Rev. Lett. **68**, 1061 (1992).
[27] C. H. Chen, S.-W. Cheong, and A. S. Cooper, Phys. Rev. Lett. **71**, 2461 (1993).
[28] S.-W. Cheong *et al.*, Phys. Rev. B **49**, 7088 (1994).
[29] S.-W. Cheong *et al.*, Phys. Rev. Lett. **67**, 1791 (1991).
[30] T. E. Mason, G. Aeppli, and H. A. Mook, Phys. Rev. Lett. **68**, 1414 (1992).
[31] T. R. Thurston *et al.*, Phys. Rev. B **46**, 9128 (1992).
[32] N. Bulut, D. Hone, D. J. Scalapino, and N. E. Bickers, Phys. Rev. Lett. **64**, 2723 (1990).
[33] J. P. Lu, Q. Si, J. H. Kim, and K. Levin, Phys. Rev. Lett. **65**, 2466 (1990).
[34] P. B. Littlewood, J. Zaanen, G. Aeppli, and H. Monien, Phys. Rev. B **48**, 487 (1993).
[35] F. Mila and T. M. Rice, Physica C **157**, 561 (1989).
[36] B. Shastry, Phys. Rev. Lett. **63**, 1288 (1989).
[37] R. E. Walstedt, B. S. Shastry, and S.-W. Cheong, Phys. Rev. Lett. **72**, 3610 (1994).
[38] V. Barzykin, D. Pines, and D. Thelen, Phys. Rev. B **50**, 16052 (1994).
[39] A. R. Moodenbaugh *et al.*, Phys. Rev. B **38**, 4596 (1988).
[40] J. D. Axe *et al.*, Phys. Rev. Lett. **62**, 2751 (1989).
[41] J. M. Tranquada, B. J. Sternlieb, J. D. Axe, Y. Nakamura, and S. Uchida, Nature (to be published).